phase, nuclear export signals in vertebrate cyclin B1 keep it out of the nucleus, and Wee1/Myt1-mediated inhibitory phosphorylation of Cdk1 maintains a low level of kinase activity until S phase is complete. These controls presumably evolved to increase the fidelity with which the genome is replicated and segregated to daughter cells. Avoiding premature entry into mitosis is vital, especially if initiation of M phase prevents completion of S phase, as seems to be the case in vertebrate cells (*29*). The nuclear export–imposed block on Cdk1–cyclin B1 supporting replication extends the range of situations in which the localization of Cdk-cyclins has been shown to influence their function (*7*). Localization determinants on the budding yeast G_1 cyclins Cln2 and Cln3 contribute to their different functions (*30*), as do the respective microtubule- and Golgi-targeting N termini of human cyclins B1 and B2 (*31*). Although differences in substrate specificity between different Cdk-cyclin complexes undoubtedly do exist (*7*), our results suggest that access to substrates in time and space plays a critical role in determining the function of particular Cdk-cyclin complexes.

References and Notes

1. P. K. Jackson, S. Chevalier, M. Philippe, M. W. Kirschner, *J. Cell Biol.* **130**, 755 (1995).
2. U. P. Strausfeld *et al.*, *J. Cell Sci.* **109**, 1555 (1996).
3. S. B. Haase, S. I. Reed, *Nature* **401**, 394 (1999).
4. A. Amon, S. Irniger, K. Nasmyth, *Cell* **77**, 1037 (1994).
5. D. L. Fisher, P. Nurse, *EMBO J.* **15**, 850 (1966).
6. B. Stern, P. Nurse, *Trends Genet.* **12**, 345 (1996).
7. M. E. Miller, F. R. Cross, *J. Cell Sci.* **114**, 1811 (2001).
8. P. R. Clarke, D. Leiss, M. Pagano, E. Karsenti, *EMBO J.* **11**, 1751 (1992).
9. M. J. Solomon, M. Glotzer, T. H. Lee, M. Philippe, M. W. Kirschner, *Cell* **63**, 1013 (1990).
10. J. R. Pomerening, E. D. Sontag, J. E. Ferrell, *Nature Cell Biol.* **5**, 346 (2003).
11. J. Pines, T. Hunter, *J. Cell Biol.* **115**, 1 (1991).
12. J. Gautier, J. L. Maller, *EMBO J.* **10**, 177 (1991).
13. J. Yang *et al.*, *Genes Dev.* **12**, 2131 (1998).
14. J. D. Moore, S. Kornbluth, T. Hunt, *Mol. Biol. Cell* **13**, 4388 (2002).
15. Materials and methods, including details of the protocol for assaying replication and the DNA constructs used in this study, are available as supporting material on *Science* Online.
16. J. D. Moore, J. A. Kirk, T. Hunt, unpublished data.
17. F. Toyoshima, T. Moriguchi, A. Wada, M. Fukuda, E. Nishida, *EMBO J.* **17**, 2728 (1998).
18. A. Hagting, C. Karlsson, P. Clute, M. Jackman, J. Pines, *EMBO J.* **17**, 4127 (1998).
19. J. D. Moore, J. Yang, R. Truant, S. Kornbluth, *J. Cell Biol.* **144**, 213 (1999).
20. D. Kalderon, B. L. Roberts, W. D. Richardson, A. E. Smith, *Cell* **39**, 499 (1984).
21. P. R. Mueller, T. R. Coleman, W. G. Dunphy, *Mol. Biol. Cell* **6**, 119 (1995).
22. P. R. Mueller, T. R. Coleman, A. Kumagai, W. G. Dunphy, *Science* **270**, 86 (1995).
23. T. Izumi, J. L. Maller, *Mol. Biol. Cell* **4**, 1337 (1993).
24. W. Chen, M. Wilborn, J. Rudolph, *Biochemistry* **39**, 10781 (2000).
25. N. Furuno, N. den Elzen, J. Pines, *J. Cell Biol.* **147**, 295 (1999).
26. A. Bueno, P. Russell, *Mol. Cell. Biol.* **13**, 2286 (1993).
27. E. Schwob, T. Bohm, M. D. Mendenhall, K. Nasmyth, *Cell* **79**, 233 (1994).
28. F. R. Cross, M. Yuste-Rojas, S. Gray, M. D. Jacobson, *Mol. Cell* **4**, 11 (1999).
29. R. T. Johnson, P. N. Rao, *Nature* **226**, 717 (1970).
30. M. E. Miller, F. R. Cross, *Mol. Cell Biol.* **20**, 542 (2000).
31. V. M. Draviam, S. Orrechia, M. Lowe, R. Pardi, J. Pines, *J. Cell Biol.* **152**, 945 (2001).

32. We thank J. Rudolph for the Cdc25B plasmid; J. Pines for the GST-p21N plasmid; T. Lindahl, F. Solomon, and A. Nebreda for critically reading the manuscript; and members of the Cell Cycle Control laboratory at Clare Hall for their encouragement and support during this work. We are especially grateful to H. Mahbubani for taking care of the frogs. Funded by Cancer Research UK.

Supporting Online Material
www.sciencemag.org/cgi/content/full/300/5621/987/DC1
Materials and Methods
References

11 December 2002; accepted 8 April 2003

Asymmetrical Allocation of NMDA Receptor ε2 Subunits in Hippocampal Circuitry

Ryosuke Kawakami,[1]* Yoshiaki Shinohara,[2]* Yuichiro Kato,[3] Hiroyuki Sugiyama,[3] Ryuichi Shigemoto,[2,4] Isao Ito[3]†

Despite its implications for higher order functions of the brain, little is currently known about the molecular basis of left-right asymmetry of the brain. Here we report that synaptic distribution of *N*-methyl-D-aspartate (NMDA) receptor GluRε2 (NR2B) subunits in the adult mouse hippocampus is asymmetrical between the left and right and between the apical and basal dendrites of single neurons. These asymmetrical allocations of ε2 subunits differentiate the properties of NMDA receptors and synaptic plasticity between the left and right hippocampus. These results provide a molecular basis for the structural and functional asymmetry of the mature brain.

The NMDA receptor plays important and diverse roles in a number of brain functions (*1*). It is composed of hetero-oligomers of GluRζ (NR1), GluRε (NR2), and, occasionally, GluRχ (NR3) subunits (*2*, *3*). The ε subunit family contains four distinct subtypes, ε1 to ε4 (NR2A to -2D). Because the four ε subunits differ in distribution and development in the brain, the subunit compositions of the NMDA receptors also differ depending on the brain regions and developmental stages (*4*–*7*). The actual subunit composition of the NMDA receptors in vivo is not known at present. NMDA receptors with distinct subunit combinations differ in physiological and pharmacological properties (*5*, *8*–*11*). Recent studies suggested the possibility that NMDA receptors with distinct properties are distributed to the synapses in an input-selective manner (*12*, *13*).

The adult mouse hippocampus expresses three distinct NMDA receptor subunits (ζ1, ε1, and ε2) (*4*, *6*, *7*). Hippocampal CA1 pyramidal neurons receive major excitatory inputs from Schaffer collateral (sch) fibers originating from ipsilateral CA3 pyramidal neurons and commissural (com) fibers, from contralateral CA3 pyramidal neurons (*14*). To characterize the NMDA receptors selectively in the sch-CA1 pyramidal neuron (sch-CA1) synapses, we have developed a method by which com fibers are denervated in live mice. Electrophysiological and immunoblot analyses using hippocampal slices from the com fiber–denervated mice revealed unexpected asymmetries in NMDA receptor–mediated responses and synaptic allocation of ε2 subunits in the hippocampus.

The bilateral hippocampi are connected by the ventral hippocampal commissure (VHC), and com fibers innervate contralateral hippocampal neurons via the VHC (*14*). We transected the VHC, thereby denervating com fibers (*15*). Selective denervation of com fibers was confirmed by the lack of retrograde transportation of the fluorescent dye, Fast blue (Fig. 1A), and by measuring the monosynaptic field excitatory postsynaptic potentials (fEPSPs) evoked on the basal dendrites of CA3 pyramidal neurons (Fig. 1B). In hippocampal slices from VHC transected (VHCT) mice 5 days after surgery, electrical stimulation at the *stratum oriens* of area CA3 evoked fEPSPs and presynaptic fiber volleys (PFVs), indicating that associational (asc) fiber-synapses on the basal dendrites of CA3 pyramidal neurons are functional in VHCT slices (VHCT and Ori, Fig. 1B). Electrical

[1]Department of Molecular Biology, Graduate School of Medical Science, Kyushu University, Fukuoka 812-8582, Japan. [2]Division of Cerebral Structure, National Institute for Physiological Sciences, School of Life Science, The Graduate University for Advanced Studies, Okazaki 444-8585, Japan. [3]Department of Biology, Faculty of Sciences, Kyushu University, Fukuoka 812-8581, Japan. [4]CREST Japan Science and Technology Corporation, Kawaguchi, Japan.

*These authors contributed equally to this work.
†To whom correspondence should be addressed. E-mail: isitoscb@mbox.nc.kyushu-u.ac.jp

stimulation in the ventral fimbria at the same or much higher intensity elicited no measurable fEPSP or PFV, indicating that com fibers were essentially nonfunctional in the VHCT mice (VHCT and Fim, Fig. 1B). In the experiments that follow, we used hippocampal slices prepared from VHCT mice 5 days after surgery.

We characterized NMDA EPSCs at the CA1 pyramidal neuron synapses using Ro 25-6981, an ε2 subunit–selective antagonist (*16*–*18*). To record NMDA EPSCs, whole-cell recordings were made from CA1 pyramidal neurons in the presence of 6,7-dinitroquinoxaline-2,3-dione (DNQX, 20 μM) and bicuculline (30 μM) at a holding potential of +10 mV (Fig. 2). Because excitatory synapses on CA1 pyramidal neurons are located on both apical and basal dendrites, NMDA EPSCs were independently elicited by electrical stimuli applied either at the *stratum radiatum* or at the *stratum oriens* of area CA1.

Figure 2A illustrates the results obtained with the stimulation at the *stratum radiatum*. In naïve mice, Ro 25-6981 (0.6 μM) reduced peak amplitudes of NMDA EPSCs to a similar extent in the left and right hippocampal slices (left, 64 ± 7% of control, $n = 5$ slices from 5 animals; right, 63 ± 4% of control, $n = 5$ from 5 animals; $P > 0.90$, t test) (Naïve, Fig. 2A). By contrast, in VHCT mice, Ro 25-6981 reduced NMDA EPSCs in the left hippocampal slices more intensely than it did in the right (left, 39 ± 3% of control, $n = 5$ from 4 animals; right, 81 ± 8% of control, $n = 5$ from 5 animals; $P < 0.01$) (VHCT, Fig. 2A). Perforant path (pp) fibers from entorhinal cortex form synapses on CA1 pyramidal neurons in the *stratum lacunosum moleculare* (*14*) and pp-CA1 synaptic responses are suppressed by the activation of presynaptic group II metabotropic glutamate receptors (mGluRs) expressed in these fibers

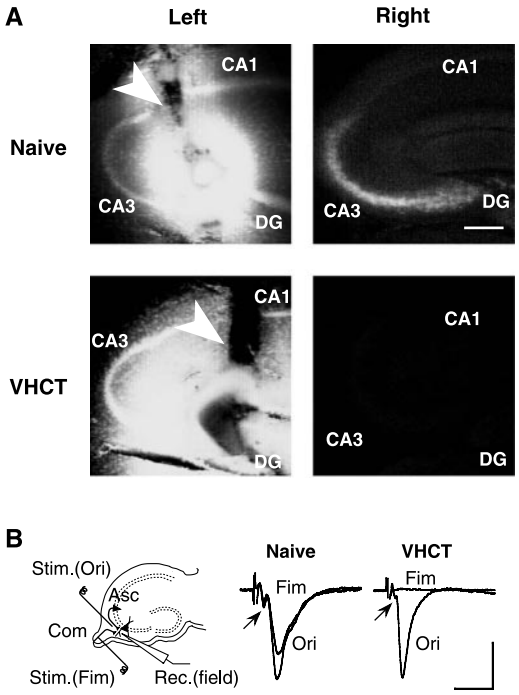

Fig. 1. Selective denervation of commissural fibers by VHC transection. (**A**) Fluorescence photomicrographs of hippocampal slices prepared from a naïve mouse (Naïve) and from a VHCT mouse (VHCT) injected with the fluorescent dye, Fast blue, into the left hippocampus (arrowheads). Retrograde labeling of the right CA3 pyramidal neurons was absent in the VHCT mouse. CA1, field CA1; CA3, field CA3; DG, dentate gyrus. Bar, 200 μm. (**B**) Schematic diagram shows synaptic inputs on the basal dendrites of a CA3 pyramidal neuron and the electrode arrangement. A stimulating electrode was placed in the *stratum oriens* of area CA3 [Stim.(Ori)] or in the ventral fimbria [Stim.(Fim)], and an extracellular electrode [Rec.(field)] was placed in the *stratum oriens* of area CA3. Asc, associational fibers; Com, commissural fibers. Sample superimposed traces show fEPSPs and PFVs (arrows) in response to electrical stimulation at the *stratum oriens* (Ori) and at ventral fimbria (Fim), respectively. Each trace is the average of three consecutive responses recorded in hippocampal slices from a naïve mouse and from a VHCT mouse 5 days after the surgery. Bars are 1.0 mV (vertical) and 10 ms (horizontal).

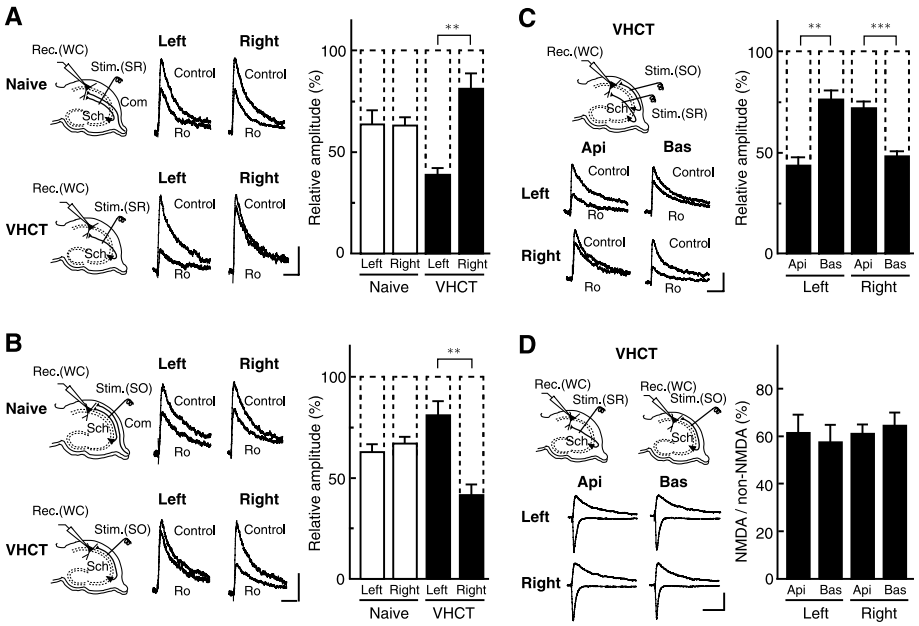

Fig. 2. Inhibitory effects of Ro 25-6981 on NMDA EPSCs in the left and right CA1 pyramidal neuron synapses. (**A**) Schematic diagrams show synaptic inputs on the apical dendrites of CA1 pyramidal neurons and arrangement of electrodes. In slices from naïve mice and from VHCT mice, electrical stimulation was applied at the *stratum radiatum* [Stim.(SR)] of area CA1. Sch, schaffer collateral fibers; Com, commissural fibers. Whole-cell recordings [Rec.(WC)] were made from CA1 pyramidal neurons. Sample superimposed traces show NMDA EPSCs recorded in the absence (Control) and presence of Ro 25-6981 (Ro, 0.6 μM). The levels of inhibition were maximal after exposure to Ro 25-6981 for 40 to 50 min (fig. S1). Left and Right indicate recordings in the left and right hippocampal slices, respectively. Each trace is the average of five consecutive recordings. Bars are 25 pA (vertical) and 100 ms (horizontal). Relative amplitudes of NMDA EPSCs in the presence of Ro 25-6981 were expressed as percentages of control responses. Columns and error bars represent means and SEM, respectively ($n = 5$ each, $^{**}P < 0.01$, absence of an asterisk indicates $P > 0.05$). (**B**) Effects of Ro 25-6981 on NMDA EPSCs evoked on the basal dendrites of CA1 pyramidal neurons. Electrical stimulation was applied at the *stratum oriens* [Stim.(SO)] of area CA1. The others are the same as those described in (A) ($n = 5$ each, $^{**}P < 0.01$, absence of an asterisk indicates $P > 0.05$). Bars are 25 pA and 100 ms. (**C**) Differential Ro 25-6981 sensitivities between apical (Api) and basal (Bas) dendrite synapses examined in the same CA1 pyramidal neuron. Using VHCT slices, electrical stimuli were applied alternately to the *stratum oriens* [Stim.(SO)] and to the *stratum radiatum* [Stim.(SR)] every 5 s. The others are the same as in (A) (for both left and right, $n = 5$ from 5 animals, $^{**}P < 0.01$, $^{***}P < 0.001$). Bars are 25 pA and 100 ms. (**D**) Ratios of NMDA EPSCs to non-NMDA EPSCs evoked on the apical and basal dendrites of CA1 pyramidal neurons in VHCT slices. Upward and downward responses in each superimposed trace are NMDA EPSC and non-NMDA EPSC, respectively. Each trace is the average of five consecutive recordings. Bars are 50 pA, 100 ms. The others are the same as in (A) and (B) ($n = 5$ each, absence of an asterisk indicates $P > 0.05$).

(*19–22*). Application of the group II selective mGluR agonist L-CCG-1 (20 μM) did not depress EPSCs evoked by stimulation at the *stratum radiatum* of area CA1 (102 ± 7% of control, $n = 5$ from 5 animals), verifying that the currents were not significantly contaminated by pp inputs.

An opposite asymmetrical effect was observed in response to stimulation at the *stratum oriens* (Fig. 2B). In naïve mice, Ro 25-6981 diminished NMDA EPSCs to the same extent in the left and right slices (left, 63 ± 4% of control, $n = 5$ from 5 animals; right, 67 ± 3% of control, $n = 5$ from 4 animals, $P > 0.40$) (Fig. 2B), whereas in the VHCT mice its effect was a mirror-image asymmetry of that found with stimulation at the *stratum radiatum* (left, 81 ± 7% of control $n = 5$ from 4 animals; right, 42 ± 5% of control, $n = 5$ from 5 animals, $P < 0.01$) (Fig. 2B).

The asymmetrical effect of Ro 25-6981 at the apical and basal dendrite synapses in VHCT slices was confirmed in the same CA1 pyramidal neurons (left apical, 43 ± 4% of control, left basal, 76 ± 5% of control, $n = 5$ from 5 animals, $P < 0.01$; right apical, 72 ± 3% of control, right basal, 48 ± 2% of control, $n = 5$ from 5 animals, $P < 0.001$) (Fig. 2C). The amplitude ratios of NMDA EPSCs to DNQX-sensitive non-NMDA EPSCs, evoked at the same stimulation intensity, were indistinguishable between these synapses in VHCT mice (left apical, 62 ± 7%, $n = 5$ from 4 animals, left basal, 57 ± 7%, $n = 5$ from 4 animals; right apical, 61 ± 4%, $n = 5$ from 4 animals, right basal, 64 ± 6%, $n = 5$ from 5 animals) (Fig. 2D). Therefore, the asymmetry observed in VHCT slices appears to be specific to the ε2 subunit–mediated component rather than to the whole NMDA current.

In VHCT slices, NMDA EPSCs evoked by electrical stimuli at the *stratum radiatum* and at the *stratum oriens* are attributable to the sch-CA1 synapses. Thus, our results indicate that Ro 25-6981 sensitivities of NMDA EPSCs in the sch-CA1 synapses are asymmetrical between the left and right hippocampus and between the apical and basal dendrites of single neurons. Subsequently, Ro 25-6981 sensitivities of NMDA EPSCs in the com-CA1 synapses are expected to have opposite asymmetries to those in the sch-CA1 synapses, because Ro 25-6981 sensitivity in naïve mice that have both sch- and com-CA1 synapses was apparently identical between the left and right hippocampus (Fig. 2, A and B). Because it is not possible to stimulate com fibers selectively in area CA1, we examined Ro 25-6981 sensitivities of NMDA EPSCs in the com fiber synapses formed on the basal dendrites of CA3 pyramidal neurons by stimulating the ventral fimbria in hippocampal slices from naïve mice. To reduce contamination of com fiber responses on the apical dendrites of CA3 pyramidal neurons and to avoid antidromic activation of ipsilateral CA3 axons by stimulation at the ventral fimbria, we optimized the cutting angles for preparation of hippocampal slices (*15*). In hippocampal slices prepared with our procedure, we confirmed that electrical stimulation at the ventral fimbria rarely induced fEPSPs and antidromic population spikes in the *stratum radiatum* and *stratum pyramidale* of area CA3, respectively. When multiple peaks in EPSCs were generated by stimulation at the ventral fimbria, we rejected the slices.

With the ventral fimbria stimulation, Ro 25-6981 reduced NMDA EPSCs in the left hippocampal slices more intensely than it did in the right (left, 43 ± 6% of control, $n = 6$ from 6 animals; right, 85 ± 7% of control, $n = 6$ from 6 animals, $P < 0.01$) (Com, Fig. 3, A and B). Half of these experiments ($n = 3$ each) were performed in a "blind" fashion, and data were pooled because results were not significantly different (left, $P > 0.75$; right, $P > 0.85$) between the blind and non-blind experiments. The amplitudes of NMDA EPSCs, estimated by the NMDA/non-NMDA EPSC ratios, were comparable between the left and right hippocampus (left, 44 ± 4%, $n = 9$ from 9 animals; right, 48 ± 5%, $n = 9$ from 8 animals, $P > 0.47$) (Fig. 3C). By contrast, when we applied electrical stimuli at the *stratum oriens* of area CA3 and activated both com and asc fibers, Ro 25-6981 sensitivity of NMDA EPSCs was apparently identical between the left and right hippocampus (left, 67 ± 10%, $n = 5$ from 5 animals; right, 60 ± 3%, $n = 5$ from 5 animals, $P > 0.5$) (Asc/Com, Fig. 3, A and B). This result further supported the assumption that we selectively activated com fibers with the ventral fimbria stimulation without significant contamination of asc inputs. Thus, the left-right asymmetry in the effect of Ro 25-6981 was also present at the synapses formed by com fibers in an opposite manner to that found at

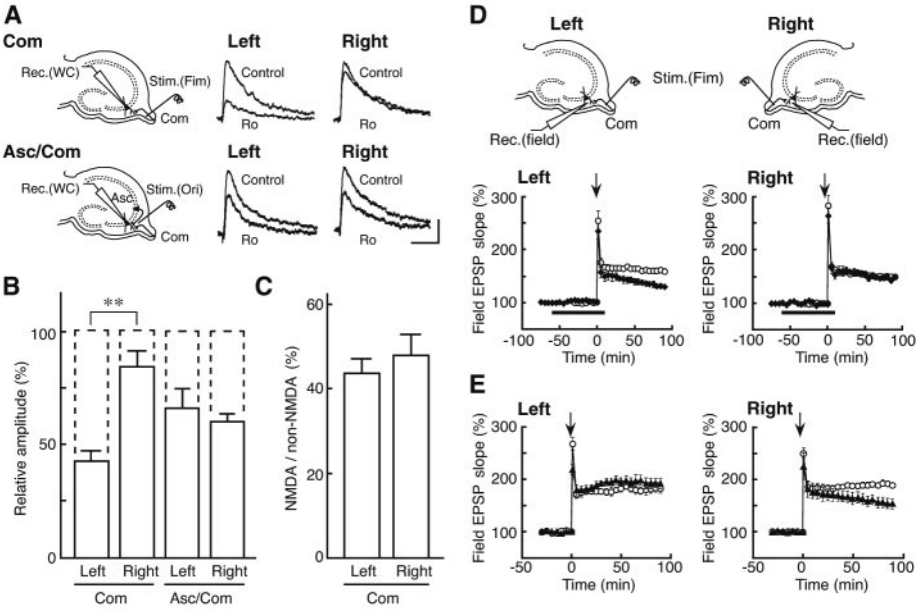

Fig. 3. Left-right asymmetry of com-CA3 synapses. (**A**) Effects of Ro 25-6981 on NMDA EPSCs in the left and right com-CA3 synapses. Schematic diagrams show synaptic inputs on the basal dendrites of CA3 pyramidal neurons and arrangement of electrodes. In slices from naïve mice, whole-cell recordings were made from CA3 pyramidal neurons. A stimulating electrode was placed in the ventral fimbria or in the *stratum oriens* of area CA3 to activate com fibers or to activate both associational and commissural fibers (Asc/Com), respectively. Superimposed traces show NMDA EPSCs recorded in the absence and presence of Ro 25-6981 (Ro, 0.6 μM). Bars are 25 pA, 100 ms. Each trace is the average of five consecutive recordings. (**B**) Relative amplitudes of NMDA EPSCs in the presence of Ro 25-6981 are expressed as percentages of the control responses. Columns and error bars represent means and SEM, respectively (Com, $n = 6$ each, $^{**}P < 0.01$; Asc/Com, $n = 5$ each, absence of an asterisk indicates $P > 0.05$). (**C**) Ratios of NMDA EPSCs to non-NMDA EPSCs in the left and right com-CA3 synapses. Columns and error bars represent means and SEM, respectively ($n = 9$ each, absence of an asterisk indicates $P > 0.05$). (**D**) Effects of Ro 25-6981 on LTPs in the left and right com-CA3 synapses. Schematic diagrams show arrangement of electrodes for extracellular recording. fEPSPs were recorded by an extracellular electrode placed in the *stratum oriens* of area CA3 and electrical stimuli were applied at ventral fimbria. A tetanic stimulation (arrows) was given in the presence (closed diamonds) and absence (open circles) of Ro 25-6981 (0.2 μM). Ro 25-6981 was applied to the bath from 60 min before the tetanic stimulation to 10 min after (thick bars). Symbols and error bars represent means and SEM, respectively ($n = 6$ to 10). (**E**) Developmental asymmetry in LTPs at the left and right com-CA3 synapses. Experimental conditions were the same as those described in (D). Open circles represent 9W mice, and filled triangles represent 2W mice. Symbols and error bars represent means and SEM, respectively ($n = 5$ to 7).

the synapses formed by sch fibers (Fig. 2B).

To examine how this asymmetrical property of NMDA receptors is reflected in the property of synaptic plasticity, we examined the effect of Ro 25-6981 on long-term potentiation (LTP) at these synapses. Similar to Ro 25-6981 sensitivities of NMDA EPSCs, LTP at the left com-CA3 synapses was significantly reduced by Ro 25-6981 (0.2 μM) (relative fEPSP slope 90 min after tetanic stimulation were as follows: control, 158 ± 2%, $n = 8$ from 8 animals; Ro, 130 ± 2%, $n = 10$ from 10 animals, $P < 0.001$) (Fig. 3D), but LTP at the right com-CA3 synapses was apparently unaffected (control, 151 ± 5%, $n = 6$ from 5 animals; Ro, 151 ± 3%, $n = 6$ from 6 animals, $P > 0.90$) (Fig. 3D). To further confirm the asymmetrical contribution of ε2 subunits to LTP, we also examined LTP in 2-week-old (2W) mice and compared it with LTP in 9-week-old (9W) mice. The ε2 subunit is the major ε subunit in the hippocampus of 2W mice (*23*). LTP in 2W mice was completely suppressed by Ro 25-6981 in both the left and right com-CA3 synapses (left, 99 ± 2 %, $n = 5$ from 5 animals; right, 101 ± 6 %, $n = 5$ from 5 animals). In the left com-CA3 synapse, the amplitudes of LTP were similar between 2W and 9W mice (2W mice, 192 ± 10 %, $n = 6$ from 6 animals; 9W mice, 182 ± 9 %, $n = 5$ from 4 animals, $P > 0.46$) (Fig. 3E). In the right com-CA3 synapse, however, the amplitude of LTP in 2W mice was smaller than that in 9W mice (2W mice, 154 ± 10 %, $n = 6$ from 6 animals; 9W mice, 189 ± 5 %, $n = 7$ from 6 animals, $P < 0.01$) (Fig. 3E), consistent with the smaller degree of contribution of ε2 subunits to LTP in the right.

The preceding observations were complemented by quantitative measurements of ε2 and ζ1 subunits in postsynaptic density (PSD) fraction (*24*) purified from the left and right CA1 *stratum radiatum* and *stratum oriens* dissected from VHCT slices. In these preparations, remaining synapses should be mostly made by heavily innervating sch fibers (*14*), though in the *stratum oriens* some weak innervation is made by axon collaterals from CA1 pyramidal cells (*14*).

In both the *stratum radiatum* and *stratum oriens*, total amounts of ζ1 and ε2 subunits in the homogenate were equal between the left and right hippocampus (Fig. 4A). In PSD fractions, however, we found a significantly higher quantity of ε2, but not ζ1 subunit in the left *stratum radiatum* than in the right and, conversely, in the right *stratum oriens* than in the left (Fig. 4A). In naïve mice, no significant difference was detected for ε2 and ζ1 subunits between PSD fractions from the left and right *stratum radiatum* (fig. S2) (Supporting Online Material Text).

On the basis of the asymmetrical allocation of ε2 subunits, hippocampal synapses formed by the inputs from CA3 pyramidal neurons are classified into two populations: one where the ε2 subunit is dominant, and the other where it is not. These two populations of synapses are considered to be located asymmetrically on pyramidal neurons (Fig. 4B). Because these populations, with complementary properties formed by ipsilateral and contralateral inputs, are located together on both the apical and basal dendrites of pyramidal neurons, it is not possible to detect asymmetrical distribution of ε2 subunits without stimulation selective to ipsilateral or contralateral input. One intriguing property of our model is its input-side selective arrangement of the ε2-dominant and ε2-nondominant synapses. For example, axons from the left CA3 pyramidal neurons (red lines, Fig. 4B) form ε2-dominant synapses (closed circles) on the apical dendrites of pyramidal neurons in bilateral hippocampi. By contrast, axons from the right CA3 pyramidal neurons (blue lines) form ε2-dominant synapses on the basal dendrites of pyramidal neurons in bilateral hippocampi. This organization might allow postsynaptic neurons to identify the side of the input source, especially in animals during the early developmental period in which the two populations of synapses differ in their ability to express NMDA receptor–dependent synaptic plasticity (Fig. 3E).

Mechanisms for generating such asymmetrical allocation of ε2 subunits may be explained by two distinct hypotheses, based on the differing properties of presynaptic and postsynaptic pyramidal neurons. First, presynaptic signals characterizing the left and right CA3 pyramidal neurons may have opposite properties for recruiting ε2 subunits in postsynaptic pyramidal neurons. Second, left and right postsynaptic pyramidal neurons may have opposite properties for sorting ε2 subunits into synapses, depending on the identities of ipsilateral or contralateral inputs and apical or basal dendrites. In either case, generation of the asymmetry requires interaction between presynaptic and postsynaptic elements originating from left and right pyramidal neurons with distinct properties.

Although the exact subunit compositions of NMDA receptors in the adult hippocampus are not clear at present, the asymmetrical allocation of ε2 subunits seems to differentiate the subtype but not the total number of NMDA receptors between these synapses, because the amount of ζ1 subunits and the amplitudes of NMDA EPSCs, estimated by the NMDA/non-NMDA EPSC ratios, are apparently identical between the left and right. By contrast, the developmental asymmetry observed in LTP at com-CA3 synapses can be explained by the difference in the number of functional NMDA receptors in these synapses. In early postnatal animals such as 2W mice, the expression of ε1 subunits in the

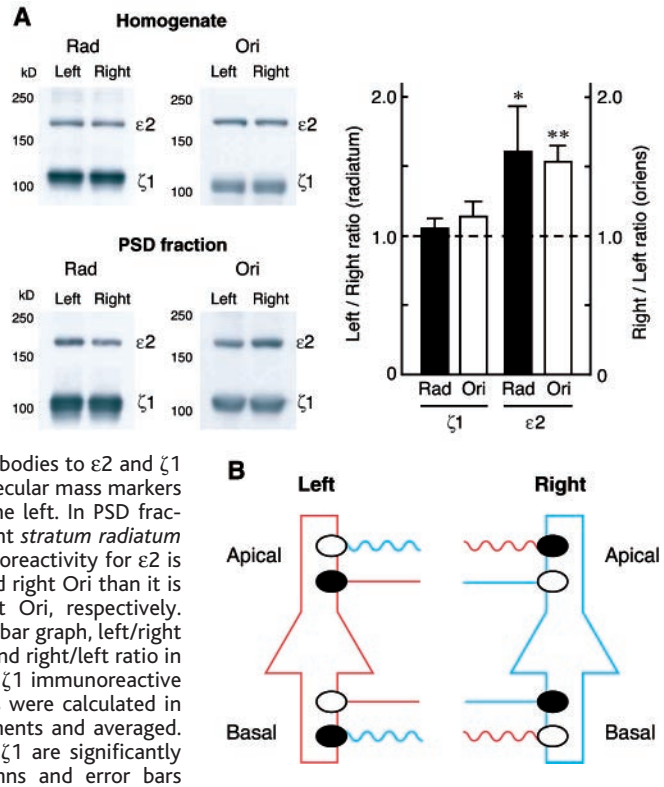

Fig. 4. Asymmetrical distribution of ε2 subunits in hippocampal synapses. (**A**) Western blot analyses of ε2 subunit proteins in sch-CA1 synapses of VHCT mice. Homogenates from the left and right *stratum radiatum* (Rad) and *stratum oriens* (Ori) of the CA1 area were blotted to PVDF membranes, and each membrane was separated into two parts including proteins larger and smaller than 135 kD and were reacted with antibodies to ε2 and ζ1 subunits, respectively. Molecular mass markers are indicated (in kD) on the left. In PSD fractions from the left and right *stratum radiatum* and *stratum oriens*, immunoreactivity for ε2 is stronger in the left Rad and right Ori than it is in the right Rad and left Ori, respectively. Ratios of optical densities (bar graph, left/right ratio in *stratum radiatum* and right/left ratio in *stratum oriens*) for ε2 and ζ1 immunoreactive bands in the PSD fractions were calculated in three independent experiments and averaged. The ratios for ε2 but not ζ1 are significantly different from 1.0. Columns and error bars represent means and SD, respectively ($n = 3$ each, $^*P < 0.05$, $^{**}P < 0.01$, *t* -test). (**B**) Hippocampal asymmetry proposed here. Left and right pyramidal neurons and their axons are colored red and blue, respectively. Closed and open circles represent ε2-dominant and ε2-nondominant synapses, respectively. Straight and wavy lines represent inputs from the ipsilateral and contralateral CA3 pyramidal neurons, respectively. Apical, apical dendrites; basal, basal dendrites.

hippocampus is still absent or low, whereas the ε2 and ζ1 subunits are already expressed at a high level (*4*, *6*, *7*, *23*). In this case, the asymmetrical allocation of ε2 subunits may produce distinct numbers of NMDA receptors in these synapses, resulting in differential ability to express synaptic plasticity (Fig. 3E). Hippocampal pyramidal neurons, thus, might regulate the development of synaptic plasticity in a side-selective manner by controlling the synaptic allocation of ε2 subunits.

The left-right asymmetry is a fundamental concept of brain science (*25*–*27*). Our present findings suggest that the brain can involve asymmetries not only at a macroscopic level of left and right hemispheres but also at microscopic levels of neurons and synapses, and they may provide an initial step for elucidating the molecular basis of brain asymmetry.

References and Notes

1. H. Mori, M. Mishina, *Neuropharmacology* **34**, 1219 (1995).
2. S. Cull-Candy, S. Brickley, M. Farrant, *Curr. Opin. Neurobiol.* **11**, 327 (2001).
3. M. Hollmann, in *Ionotropic Glutamate Receptors in the CNS*, P. Jonas, H. Monyer, Eds. (Springer, Berlin, 1999), pp. 1–98.
4. H. Monyer, N. Burnashev, D. J. Laurie, B. Sakmann, P. H. Seeburg, *Neuron* **12**, 529 (1994).
5. H. Monyer *et al.*, *Science* **256**, 1217 (1992).
6. M. Watanabe, Y. Inoue, K. Sakimura, M. Mishina, *Neuroreport* **3**, 1138 (1992).
7. M. Watanabe, Y. Inoue, K. Sakimura, M. Mishina, *J. Comp. Neurol.* **338**, 377 (1993).
8. G. Kohr, P. H. Seeburg, *J. Physiol.* **492**, 445 (1996).
9. T. Kutsuwada *et al.*, *Nature* **358**, 36 (1992).
10. S. Vicini *et al.*, *J. Neurophysiology* **79**, 555 (1998).
11. K. Williams, S. L. Russell, Y. M. Shen, P. B. Molinoff, *Neuron* **10**, 267 (1993).
12. K. Gottmann, A. Mehrle, G. Gisselmann, H. Hatt, *J. Neurosci.* **17**, 2766 (1997).
13. I. Ito, R. Kawakami, K. Sakimura, M. Mishina, H. Sugiyama, *Neuropharmacology* **39**, 943 (2000).
14. D. G. Amaral, M. P. Witter, in *The Rat Nervous System*, G. Paxinos, Ed. (Academic Press, San Diego, CA, 1995), pp. 443–494.
15. Materials and Methods are available as supporting material on *Science* Online.
16. B. A. Chizh, P. M. Headley, T. M. Tzschentke, *Trends Pharmacol. Sci.* **22**, 636 (2001).
17. G. Fischer *et al.*, *J. Pharmacol. Exp. Ther.* **283**, 1285 (1997).
18. V. Mutel *et al.*, *J. Neurochem.* **70**, 2147 (1998).
19. R. S. Petralia, Y. X. Wang, A. S. Niedzielski, R. J. Wenthold, *Neuroscience* **71**, 949 (1996).
20. R. Shigemoto *et al.*, *J. Neurosci.* **17**, 7503 (1997).
21. A. Contractor, G. T. Swanson, A. Sailer, S. O'Gorman, S. F. Heinemann, *J. Neurosci.* **20**, 8269 (2000).
22. J. Kilbride, L. Q. Huang, M. J. Rowan, R. Anwyl, *Eur. J. Pharmacol.* **356**, 149 (1998).
23. I. Ito, K. Sakimura, M. Mishina, H. Sugiyama, *Neurosci. Lett.* **203**, 69 (1996).
24. C. W. Cotman, D. Taylor, *J. Cell Biol.* **62**, 236 (1974).
25. M. C. Corballis, *Trends Cogn. Sci.* **2**, 152 (1998).
26. L. J. Rogers, R. J. Andrew, Eds., *Comparative Vertebrate Lateralization* (Cambridge Univ. Press, Cambridge, 2002).
27. S. P. Springer, D. Deutsch, *Left Brain, Right Brain: Perspectives from Cognitive Neuroscience* (W. H. Freeman, New York, ed. 5, 1997).

28. We thank N. Tamamaki for technical advice and comments; Hoffmann–La Roche (Nutley, New Jersey) for Ro 25-6981; M. Watanabe for antibodies; G. L. Collingridge, M. Kuno, T. Manabe, P. Somogyi and T. Takahashi for their comments on the manuscript; and M. Mishina, S. Nagae, and K. Sakimura for their advice. Supported by the Ministry of Education, Science and Culture of Japan and by the Cooperative Study Program of National Institute for Physiological Sciences.

Supporting Online Material
www.sciencemag.org/cgi/content/full/300/5621/990/DC1

Materials and Methods
SOM Text
Figs. S1 and S2

21 January 2003; accepted 8 April 2003

Eye-Specific Retinogeniculate Segregation Independent of Normal Neuronal Activity

Andrew D. Huberman,[1] Guo-Yong Wang,[2] Lauren C. Liets,[2] Odell A. Collins,[1] Barbara Chapman,[1,2]* Leo M. Chalupa[1,2,3]*

The segregation of initially intermingled left and right eye inputs to the dorsal lateral geniculate nucleus (DLGN) during development is thought to be in response to precise spatial and temporal patterns of spontaneous ganglion cell activity. To test this hypothesis, we disrupted the correlated activity of neighboring ganglion cells in the developing ferret retina through immunotoxin depletion of starburst amacrine cells. Despite the absence of this type of correlated activity, left and right eye inputs segregated normally in the DLGN. By contrast, when all spontaneous activity was blocked, the projections from the two eyes remained intermingled. Thus, certain features of normal neural activity patterns are not required for the formation of eye-specific projections to the DLGN.

In all species with highly developed binocular vision, the projections from the two eyes are segregated into separate layers within the DLGN (*1*). Early in development, however, retinogeniculate projections from the two eyes overlap (*2, 3*). For example, in the ferret, retinogeniculate inputs are intermingled extensively at birth and then gradually segregate into eye-specific layers by P10 (postnatal day 10) (*4*–*6*). During the period of eye-specific segregation, spontaneous "waves" of excitation periodically emerge and propagate across restricted domains of the retinal surface, inducing neighboring ganglion cells to fire synchronous bursts of action potentials (*7*–*10*). Because the bursts are correlated within each retina, spiking activity is highly synchronized within one eye and unsynchronized between eyes. This pattern of activity is thought to ensure that (i) neighboring ganglion cells "fire together" and thereby "wire together" onto the same DLGN neurons, and (ii) axons from ganglion cells in the two eyes that initially converge on the same DLGN cells are temporally uncorrelated in their firing, causing weakening and elimination of dual eye inputs to single DLGN neurons (*11, 12*).

Indeed, pharmacologic manipulations that eliminate all spontaneous retinal activity prevent the segregation of eye-specific inputs to the DLGN (*6, 13*), and altering the balance of retinal activity between the two eyes leads to an increase in the size of the terminal field arising from the more active eye, at the expense of the less active eye (*13, 14*). However, in every experiment where spontaneous retinal activity has been blocked, all retinal activity was abolished (*6, 13, 14*), and in the one experiment where retinal activity was elevated (*14*), correlated ganglion cell activity was maintained. Thus, although the relative level of activity in the two eyes is important for normal retinogeniculate development, it is not yet known whether normal spatiotemporal patterns of neural activity are necessary for eye-specific segregation.

During the period of eye-specific segregation, spontaneous retinal activity is driven by acetylcholine released from starburst amacrine cells (*15, 16*). To perturb this activity, we injected an immunotoxin that rapidly depletes these cells into the eye of P0 ferrets (Fig. 1) (*17*).

An efficient way to examine activity patterns across broad areas of the developing retina is to perform low-magnification optical recordings of intracellular calcium concentrations ($[Ca^{2+}]_i$) (*15*–*17*). In control (P3 to P7) ferret retinas, this revealed the presence of well-described propagating "waves." Waves appeared largely normal in the youngest toxin-treated retinas (P3 to P5). However, their intensity diminished with age, and by P6, waves were barely visible by eye. To quantify calcium levels on a local scale, we measured the amplitude and frequency of calcium transients from a restricted area within each ret-

[1]Center for Neuroscience, [2]Section of Neurobiology, Physiology and Behavior, [3]Department of Ophthalmology, School of Medicine, University of California, Davis, CA 95616, USA.

*To whom correspondence should be addressed. E-mail: bxchapman@ucdavis.edu, lmchalupa@ucdavis.edu